

Collaborative Human-Robot Exploration via Implicit Coordination

Yves Georgy Daoud, Kshitij Goel, Nathan Michael, and Wennie Tabib

Abstract—This paper develops a methodology for collaborative human-robot exploration that leverages implicit coordination. Most autonomous single- and multi-robot exploration systems require a remote operator to provide explicit guidance to the robotic team. Few works consider how to embed the human partner alongside robots to provide guidance in the field. A remaining challenge for collaborative human-robot exploration is efficient communication of goals from the human to the robot. In this paper we develop a methodology that implicitly communicates a region of interest from a helmet-mounted depth camera on the human’s head to the robot and an information gain-based exploration objective that biases motion planning within the viewpoint provided by the human. The result is an aerial system that safely accesses regions of interest that may not be immediately viewable or reachable by the human. The approach is evaluated in simulation and with hardware experiments in a motion capture arena. Videos of the simulation and hardware experiments are available at: <https://youtu.be/7jgkBpVFIoE>.

I. INTRODUCTION

State-of-the-art exploration methodologies leverage the human as an *operator* outside of the exploration environment instead of directly engaging them side-by-side with robots [1, 2, 3]. Modeling the human as a *collaborator* instead of an *operator* in a shared workspace for exploration enables more efficient distributed exploration and useful emergent robot behaviors [4]. In this work, a collaborative human-robot exploration system is developed to explore 3D unstructured environments (Fig. 1a) by communicating the field of view (FoV) of the human to the robot (Fig. 1b) and having the robot use this region of interest (ROI) to bias motion plans to acquire views of areas occluded to the human (Fig. 1c).

Explicit robot tasking is impractical [5] during time-sensitive human-robot collaborative exploration (e.g. cave search and rescue) if humans must reduce their operational tempo [6, 7, 8], so implicit communication of spatial goals is imperative. State-of-the-art exploration objectives reduce environmental uncertainty without providing the flexibility to prioritize ROIs. To address these gaps in the state of the art, this work presents a collaborative human-robot exploration system that: (1) leverages implicit communication to spatially task an aerial system to regions occluded to the human, and (2) develops an information-gain based objective function inspired by the active object reconstruction literature [9] to bias motion planning within the ROI specified by the human. The approach is evaluated with real-time simulations and real-world hardware experiments in a motion capture arena.

The authors are with the Robotics Institute, Carnegie Mellon University, Pittsburgh, PA 15213 USA (e-mail: {ydaoud,kshitij,nmichael,wtabib}@cmu.edu).



(a)



(b)



(c)

Fig. 1: (a) A human-robot team is tasked with exploring a cave. (b) The human implicitly conveys a region of interest to the robot by transmitting their current viewpoint. (c) The robot plans a path to areas of the environment that are occluded to the human.

II. RELATED WORK

This work lies at the intersection of two key areas: implicit coordination for collaborative human-robot exploration and motion planning objectives for active mapping. In this section we review and contrast related works with the method detailed in this paper.

Few prior works study implicit coordination for collaborative human-robot exploration. Govindarajan et al. [4] achieve coordination through a distributed strategy that assigns robots to homotopy classes that are complementary to the ones being traversed by the human. It is assumed that a blueprint of the environment is available to identify homotopy classes before operation. In contrast, the proposed approach does not assume prior information on the environment layout. A motion primitive-based planner is leveraged to maximize information gain, which takes the human’s view into account, and drives the robot to explore regions occluded to the human; therefore, prior environment knowledge is not required.

Within the context of multitasking, implicit communication has been used to augment human situational awareness via a robotic system. Bentz et al. [10] leverage head tracking while a human performs an arbitrary number of complex tasks and fit the data to a visual interest function. An aerial robot uses the visual interest function to provide camera views that augment the human’s situational awareness. This methodology does not directly translate to the exploration context because the visual interest function, which effectively rates the utility of a viewpoint, is difficult to specify before or during exploration. Instead, the proposed approach uses the notion of potential information gain over a discrete set of candidate viewpoints to drive the robot towards the ROI.

Reardon et al. [11] leverage augmented reality to share information between a robot and human cooperatively exploring in the field. The goal is to influence the behavior of the human teammate in the human-robot cooperative exploration task by sharing information about the robot’s current plan, the task state, and communicating future actions. In contrast, the proposed approach develops a methodology to influence the robot’s behavior depending on actions taken by the human. This implicit coordination is desirable in applications like search and rescue where the robot is expected to adapt to the human’s operational tempo.

Many motion planning objectives have been proposed for active mapping. Frontier-based objectives utilize the distance to the boundary between unknown and known space to drive the robot’s exploration [12]. For multi-agent operation, prioritization between frontiers is utilized to assign agents towards complementary regions of the environment [13]. However, deployments of this idea and its variants have been limited to multiple robots [14, 2], with the human largely supplying spatial goals explicitly when desired [15]. Further, information-theoretic objectives utilize the expected change in the entropy of the map due to candidate sensor measurements to drive viewpoint selection in both 2D [16, 17] and 3D environments [18]. While real-world operation has been shown using single [19] and multiple aerial robots [20], these techniques have not been leveraged in collaborative human-robot exploration. A key capability missing in these objectives is the ability to prioritize spatial ROIs. Towards imposing such spatial constraints, volumetric next-best-view (NBV) selection methods have been proposed for the active object reconstruction problem where the viewpoint is generated to focus on high-fidelity reconstruction of a single object [21, 22]. Delmerico et al. [9] propose several variants of information gain objectives that are either counting-based [21], probabilistic [22], or a combination. However, a method to apply these objectives in the collaborative human-robot exploration system is lacking in the literature. To this end, this work proposes and evaluates an Occlusion-Aware Volumetric Information (OAVI) objective that extends the work of Delmerico et al. [9] to the collaborative human-robot exploration problem. We further contrast it to ROI-constrained Cauchy-Schwarz Quadratic Mutual Information (ROI-CSQMI), an extension of [18] developed in this work, which applies the human’s FoV as a spatial constraint.

III. METHODOLOGY

This section details the collaborative human-robot exploration method. The human and robot incrementally build a shared map of the environment using range measurements, while the robot uses the occupancy, ROI, and distance information within the shared map for motion planning. We first describe the shared map representation.

A. Shared Map Representation

The shared map is modeled as a global 3D occupancy grid (OG) map, $\mathbf{m} = \{m_1, \dots, m_{|\mathbf{m}|}\}$. Each cell m_i contains a tuple of three scalar features: (1) the probability of occupancy (o_i), (2) a boolean indicating if the cell is in the ROI (b_i), and (3) the distance of the cell from the closest obstacle (d_i). Each cell m_i is initially presumed unknown ($o_i = 0.5$), considered outside the ROI ($b_i = 0$), and assumed to be at an infinite distance from the closest obstacle ($d_i \rightarrow \infty$). The range measurements at time t are denoted by \mathbf{z}_t^h for the human and \mathbf{z}_t^r for the robot. It is assumed that the global position and orientation of these sensors are perfectly known.

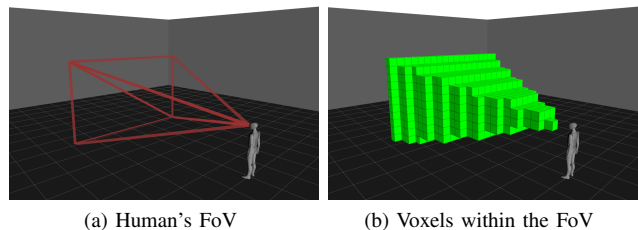


Fig. 2: (a) The human’s field of view (FoV) is shown in red and used to determine which (b) cells in the global occupancy map are within the ROI (shown in green).

For the cells within the FoVs of \mathbf{z}_t^h and \mathbf{z}_t^r , the probability of occupancy o_i is updated using the standard log-odds update [23]. However, the ROI values b_i are only set to 1 within the FoV of \mathbf{z}_t^h . The FoV is mathematically modeled using the fusion of two triangles in 2D and two tetrahedrons in 3D built from the sensor’s intrinsic matrix (see Fig. 2a). A subset of cells corresponding to inliers of the FoV are shown in Fig. 2b. This subset is extracted via inlier queries with respect to the tetrahedrons on the centers of all cells in the shared map. The distance values d_i are updated for the cells raycasted by both \mathbf{z}_t^h and \mathbf{z}_t^r with the Euclidean distance from the nearest occupied cell. We utilize the approximation by Delmerico et al. [9] that extends the rays behind a hit cell, m_{hit} , and populates the distance value at the current time, d_i^t , for the remaining raycasted cells:

$$d_i^t = \begin{cases} \|f(m_{\text{hit}}) - f(m_i)\|_2, & \text{if } \|f(m_{\text{hit}}) - f(m_i)\|_2 < d_i^{t-1} \\ d_i^{t-1}, & \text{otherwise} \end{cases} \quad (1)$$

where d_i^{t-1} is the previously stored distance in cell m_i and $f : \mathbb{Z}_+ \rightarrow \mathbb{R}^n$ is a function that converts a cell index to the cell position in the world frame. $n = 2$ or $n = 3$ depending on the dimensionality of the map representation.

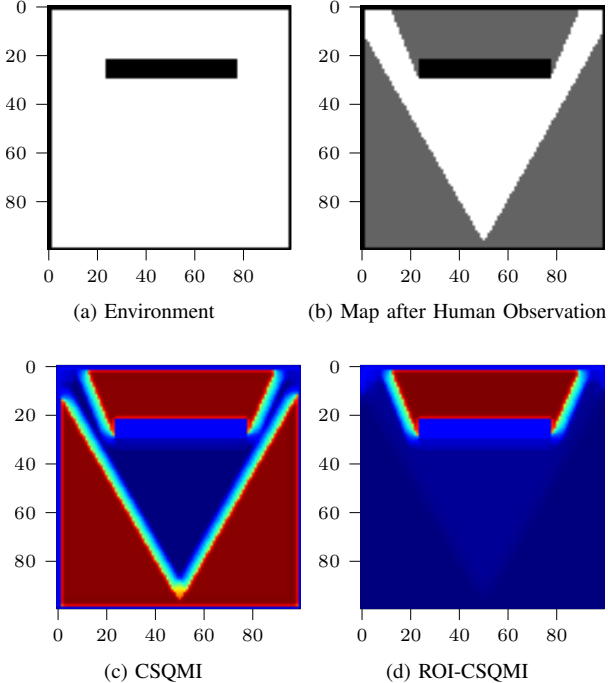


Fig. 3: Comparison of the information gain objectives using a 2D numerical example. For the environment in (a) and human at (50, 0), the map updated after one \mathbf{z}^h (Section III-A) is shown in (b). The CSQMI objective from [18] shown in (c) does not account for \mathbf{z}^h , while the ROI-CSQMI objective in (d) places higher weights in the occluded region.

After obtaining the first observation from the human and updating the shared map, the robot iteratively performs a two-step process: updating the map and selecting the next best action. The rate of this process is specified by the user prior to operation. The space of candidate actions used for action selection is generated using a library of forward-arc motion primitives for a depth camera as presented in [19]. The best primitive is chosen by maximizing the information gain over this discrete action space, which is computed at the end viewpoint of each motion primitive. We contribute one information gain objective function (OAVI) and contrast to a baseline information-theoretic objective function (CSQMI) as well as an extension of it (ROI-CSQMI) in this work.

B. ROI-constrained CSQMI (ROI-CSQMI)

The ROI-CSQMI information gain objective function modifies the CSQMI objective function proposed by Charrow et al. [18] by imposing a spatial constraint corresponding to the FoV of the range measurement from the human \mathbf{z}_t^h . The original formulation proceeds as follows; first, for a candidate viewpoint, a beam-based measurement model is used to determine which cells in the current map will be observed via raycasting. Second, the CSQMI objective is computed treating the raycasted cells independently of each other. Lastly, the CSQMI contributions from all cells are added to determine the total utility of the viewpoint. Our

contribution lies in modifying the second step using the ROI information stored in the shared map representation (Section III-A).

Let the set of cells raycasted by the candidate measurement $\hat{\mathbf{z}}_t^r$ be denoted by $\hat{\mathbf{m}}$. This set is a subset of the current map, $\hat{\mathbf{m}} \subseteq \mathbf{m}$. To impose the spatial constraint corresponding to the FoV of \mathbf{z}_t^h , we leverage the information in \mathbf{m} to obtain a new set of raycasted cells within the ROI denoted as $\hat{\mathbf{c}}$:

$$\hat{\mathbf{c}} = \{m_i \in \hat{\mathbf{m}} \mid b_i = 1, i \in \{1, \dots, |\hat{\mathbf{m}}|\}\}. \quad (2)$$

The ROI constraint is imposed at the raycasting step by finding the subset of cells that lie within the human's ROI. The CSQMI objective for the candidate measurement $\hat{\mathbf{z}}_t^r$, $I_{\text{CS}}[\hat{\mathbf{m}}; \hat{\mathbf{z}}_t^r]$, is computed using $\hat{\mathbf{m}}$ via the equations derived in [18]. Note that when $\hat{\mathbf{c}} = \hat{\mathbf{m}}$, the ROI-CSQMI objective function is equivalent to the CSQMI objective function.

For a 2D environment with an obstacle (Fig. 3a), the map \mathbf{m} is shown in Fig. 3b after adding one range measurement \mathbf{z}^h from the human who is located at the bottom center of the environment. The grey, black, and white cell colors denote unknown, occupied, and free state, respectively. Figure 3c shows the heatmap for $I_{\text{CS}}[\hat{\mathbf{m}}; \hat{\mathbf{z}}_t^r]$, which treats all unknown space equally. Figure 3d shows the heatmap for $I_{\text{CS}}[\hat{\mathbf{c}}; \hat{\mathbf{z}}_t^r]$, which prioritizes regions within the FoV of \mathbf{z}^h . The spatially constrained ROI-CSQMI objective enables implicit coordination between the human and robot during exploration by placing higher weight on views that intersect the ROI. However, there are two drawbacks to this modification: (1) the objective weighs all cells within the occluded region equally, as opposed to the regions closer to the obstacle within the human's FoV, and (2) once the robot enters the ROI during exploration, it is unlikely that it will exit it. The OAVI objective, presented next, alleviates these drawbacks.

C. Occlusion-Aware Volumetric Information (OAVI)

The proposed information-gain objective function, OAVI, is inspired by [9] and modifies the uncertainty-aware, I_{UA} , the ROI, I_{ROI} , and the proximity-aware, I_{PA} metrics.

The uncertainty-aware metric I_{UA} measures the uncertainty of the cell and accounts for potential occlusions:

$$I_{\text{UA}}(m_i) = H(m_i)P_V(m_i). \quad (3)$$

$H(m_i)$ is Shannon's entropy [24] of cell m_i , and $P_V(m_i)$ is the likelihood that the cell is visible from the current sensor pose. The result is shown in Fig. 4a for the 2D map in Fig. 3b and illustrates high weights in the unknown space.

The ROI metric, I_{ROI} , biases the objective values towards the ROI. We employ the information stored in the shared map (Section III-A) to mark the contribution of cells in the ROI towards I_{ROI} as 1. For the other regions of the map, the contribution is set to a user-specified value, $\alpha_{\text{ROI}} < 1$:

$$I_{\text{ROI}}(m_i) = \begin{cases} 1, & \text{if } b_i = 1 \\ \alpha_{\text{ROI}}, & \text{otherwise} \end{cases} \quad (4)$$

Intuitively, α_{ROI} controls the weight given to the unknown regions of the environment outside the ROI. A non-zero

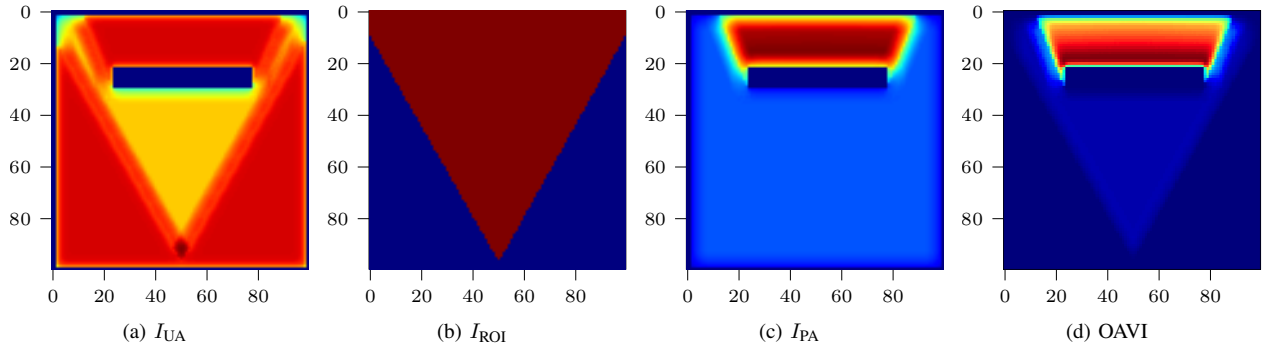


Fig. 4: Heatmaps for the OAVI objective and its constituent terms (Section III-C) over the 2D map shown in Fig. 3b. Compared to ROI-CSQMI in Fig. 3d, the OAVI objective function in Fig. 4d exhibits a gradient biasing the exploration to focus on the occluded region closer to the human’s FoV first.

α_{ROI} enables the robot to explore unknown regions after prioritizing occluded regions within the ROI. This metric is shown in Fig. 4b with $\alpha_{ROI} = 0.15$ for the 2D map in Fig. 3b.

The same modification is applied for the proximity-aware metric, I_{PA} , which utilizes the distance values, d_i , in the cells:

$$I_{PA}(m_i) = \begin{cases} d_{max} - d_i, & \text{if } o_i = 0.5 \text{ and } d_i \leq d_{max} \\ \alpha_{PA}, & \text{otherwise} \end{cases} \quad (5)$$

where d_{max} is the max sensor range, d_i is the distance from cell m_i to the closest raytraced occupied cell, and $\alpha_{PA} \in [0, 1)$ is a tunable parameter. This modification produces a gradient that places higher weights on cells close to an observed surface (e.g. see Fig. 4c where $\alpha_{PA} = 0.10$).

The final information gain I_{OAVI} is defined as the cumulative product of each metric over the raycasted cells $\hat{\mathbf{m}}$ corresponding to the robot measurement at the viewpoint $\hat{\mathbf{z}}_t^r$:

$$\begin{aligned} I_{OAVI}[\hat{\mathbf{m}}; \hat{\mathbf{z}}_t^r] &= \prod_{i \in [1, |\hat{\mathbf{m}}|]} I_{OAVI}(\hat{m}_i) \\ &= \prod_{i \in [1, |\hat{\mathbf{m}}|]} I_{UA}(\hat{m}_i) I_{ROI}(\hat{m}_i) I_{PA}(\hat{m}_i). \end{aligned} \quad (6)$$

Figure 4d illustrates the heatmap corresponding to $I_{OAVI}[\hat{\mathbf{m}}; \hat{\mathbf{z}}_t^r]$. Note the gradient behind the obstacle in OAVI, which has the effect of weighting the viewpoints that observe occluded regions more heavily, and contrast this with the uniform weighting of ROI-CSQMI in Fig. 3d.

IV. EXPERIMENTAL DESIGN AND RESULTS

The approach is evaluated in simulation and with real-world hardware experiments. The experiment begins when the human transmits the pose of their helmet-mounted range sensor with the corresponding pointcloud to the robot partner. Only one instance of these pose and pointcloud pairs is transmitted for both simulation and hardware experiments. The proposed methodology may allow for multiple pose and pointcloud pairs, but this is left as future work. When the robot receives data from the human, exploration begins.

The OAVI approach is compared against the ROI-CSQMI and CSQMI approaches. Two quantitative and one qualitative

measures are used to evaluate performance. The two quantitative evaluations measure the entropy of the map and ROI over time. The qualitative evaluation plots the evolution of the robot’s trajectory over time.

Parameter	Simulation	Hardware
Robot sensor range	5 m	2 m
Robot sensor downsampling	2×	2×
Human sensor range	10 m	6 m
Human sensor downsampling	4×	4×
Human FoV percentage	40%	30%
Mapping frequency	10 Hz	10 Hz
Voxel resolution	0.3 m	0.2 m
Grid bounding box	30 × 30 × 10 m	4 × 5 × 2 m
Planning frequency	1 Hz	1 Hz
Number of motion primitives	21	15
Max. forward velocity	0.75 m/s	0.40 m/s
Max. yaw rate	0.25 rad/s	0.25 rad/s
OAVI α_{ROI}	0.10	0.10
OAVI α_{PA}	0.15	0.15

TABLE I: List of parameter values used in the simulation and hardware experiments.

A. Simulation Experiments

Simulations in four environments (Fig. 5) are conducted to evaluate the approaches developed in this work against the baseline approach. The simulation environments consist of a single wall, two walls, multiple obstacles, and the cave environment from Fig. 1 with the same human-robot placement. In each environment the goal is for the robot to obtain views in regions occluded to the human. These environments are selected to highlight the merits and drawbacks of the information gain objectives.

In each environment, the human faces the area of interest. The human’s FoV, which is the FoV of a simulated depth camera on the human’s head, is shown as red lines in Fig. 2a. The robot is placed at a randomly selected location within a 4 × 4 m box around the human’s starting position. After the human transmits their pointcloud observation and pose to the robot, the robot updates its onboard map according to Section III-C. Each exploration variant is run for 30 trials

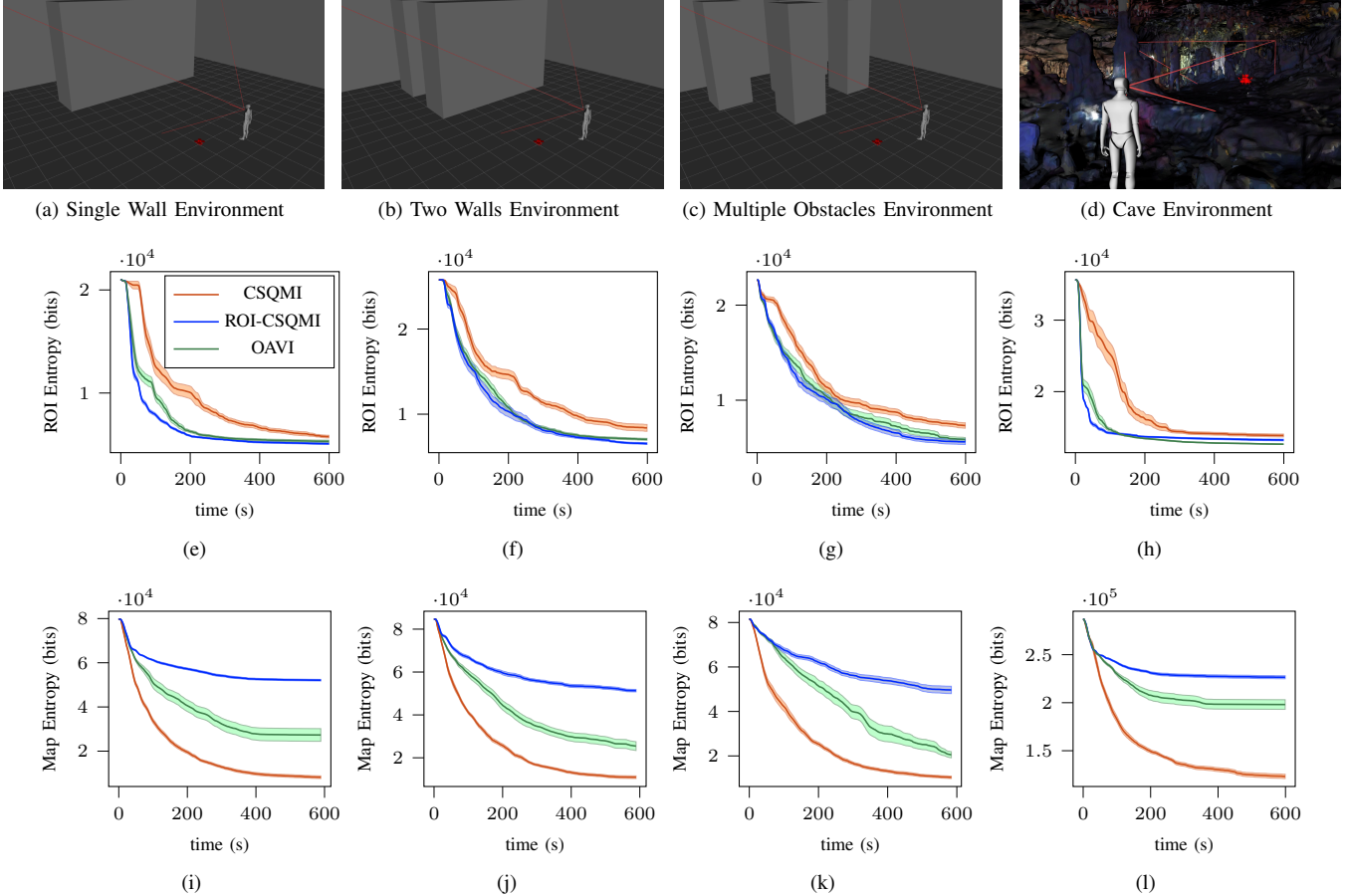


Fig. 5: (a)–(d) simulation environments, (e)–(h) ROI entropy plotted as a function of time and (i)–(l) map entropy plotted as a function of time for the CSQMI, ROI-CSQMI, and OAVI exploration variants. 30 trials are run for each exploration variant and simulation environment. Note that ROI-CSQMI and OAVI explore the human’s FoV $3\times$ faster than CSQMI while CSQMI reduces the total map uncertainty faster. OAVI reduces the map uncertainty 56% more than ROI-CSQMI.

per environment for a total of 360 trials over all environments and variants. Exploration is terminated after 10 min resulting in a total of 60 h of simulations.

The entropy of the ROI is plotted over time for each environment in Figs. 5e to 5h and the entropy of the map (including the ROI) is plotted over time in Figs. 5i to 5l. In analyzing the performance of Figs. 5e to 5h one can see that OAVI and ROI-CSQMI decrease the uncertainty of the ROI approximately $3\times$ faster than CSQMI. ROI-CSQMI slightly outperforms OAVI because the mutual information of a view entirely outside of the ROI is zero, which means that the robot will not select actions outside the ROI. In contrast, OAVI tends to drive the robot outside the ROI after sufficient views of the ROI have been acquired. When analyzing the map entropy over time in Figs. 5i to 5l, one can see that the final map entropy of the OAVI approach at 600s is on average 56% lower than the ROI-CSQMI approach across environments. The baseline CSQMI approach outperforms the other approaches because it selects views that maximize the mutual information between the map and sensor without

consideration for the ROI.

From these results, we arrive at the following conclusions: first, the baseline CSQMI approach is not well suited for collaborative human-robot exploration because it does not bias the exploration towards the ROI; second, the ROI-CSQMI approach is ideal for a leader-follower exploration strategy because it selects motion plans that are restricted within the ROI; and third, the OAVI approach is ideal for a collaborative framework where the robot biases views within the ROI first and then selects observations outside the ROI.

Figure 6 plots the top-down views of the trajectories taken by the robot for the three approaches in the two walls environment (shown in Fig. 5b). The evolution of the trajectory for $t = \{30, \dots, 60\}$ s in Fig. 6 demonstrates that OAVI first explores the occluded region closest to the human observer and then proceeds to the second obstacle after the robot has updated its distance field. In comparison, ROI-CSQMI does not incorporate a measure of the distance to obstacles so it selects actions that maximize the mutual information between the potential observation and ROI, while CSQMI

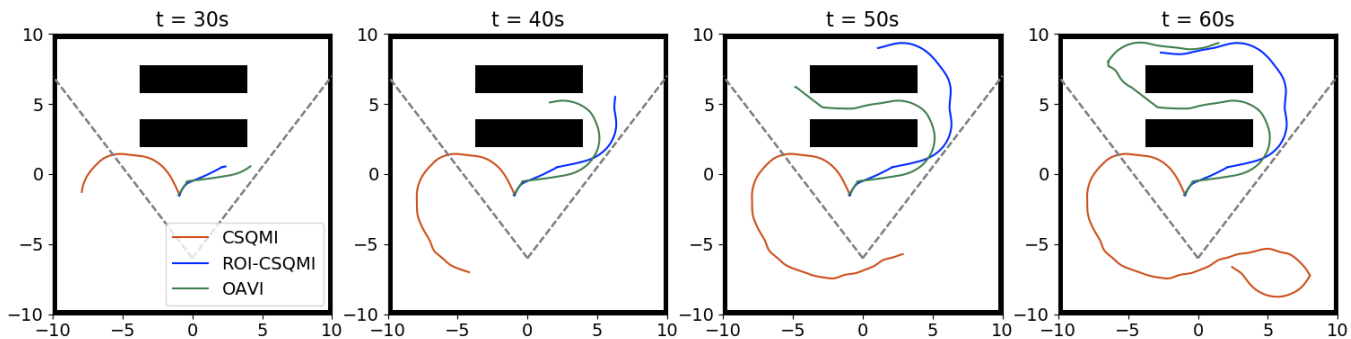


Fig. 6: Top-down snapshots of the trajectory taken by the robot for the three approaches in the two walls environment with the human’s FoV drawn in gray dashed lines. CSQMI proceeds to explore the unknown regions outside of the human’s FoV, while the ROI-constrained CSQMI and OAVI prioritize the ROI first. As opposed to ROI-CSQMI, the gradient in the OAVI approach (see Fig. 4d) pushes the robot to explore the occluded region closest to the human first.

explores areas outside of the human’s ROI for the first 60s because it does not have a notion of the human’s ROI.

B. Hardware Experiments

Experiments are run inside a motion capture arena to validate the proposed approach against the baselines in the real-world. The human is equipped with a helmet-mounted Intel RealSense D455 depth camera (see Fig. 7). The robot, a 2.5 kg quadrotor, carries a forward-facing D455 and two on-board computers: an NVIDIA TX2 running state estimation and control, and an Intel i7 NUC 11 with 32GB of RAM, which runs mapping, planning, and collision avoidance.



Fig. 7: (Left) Aerial robot and (Right) helmet for the human partner used in the hardware experiments.

The set of parameters used in the hardware experiments (see Fig. 8) are listed in Table I. Each approach is run once starting from the same initial robot pose and a fixed helmet orientation for a total time of 2 min.

The ROI and map entropy are plotted over time in Fig. 9. The baseline CSQMI approach reduces the total uncertainty in the environment fastest Fig. 9b. ROI-CSQMI explores the ROI twice as fast as OAVI, and 4× as fast as CSQMI (see Fig. 9a) but does not select actions outside of the ROI once it reaches the ROI. This behavior yields the blue plateau in the map at $t = 50$ s. In contrast, OAVI explores the rest of the unknown environment as shown in the final map (Fig. 10), reducing the map entropy by 75% more than ROI-CSQMI.

To demonstrate computational-efficiency of the proposed approach, we record the planning times taken by the action

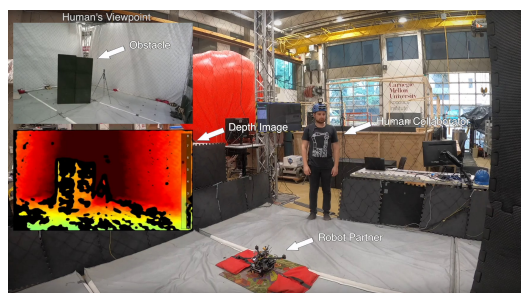


Fig. 8: A human-robot team explores an environment inside a motion capture arena, with an obstacle in front the human requiring the robot to provide complementary views.

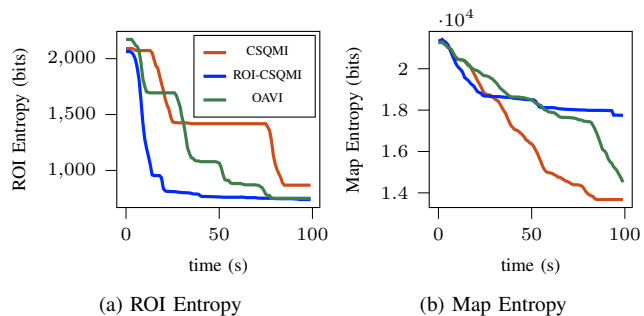


Fig. 9: ROI and map entropy as a function of time for the three approaches. The baseline CSQMI approach minimizes the total map entropy, while its extension ROI-CSQMI prioritizes the ROI. OAVI successfully reduces the uncertainty in the ROI first, followed by an exploratory behavior. A video of the experimental setup and the three exploration approaches can be found at <https://youtu.be/7jgkBpVFIoE>.

generation, scoring, and best primitive selection modules onboard the robot’s computer. The results reported in Table II show close planning times between the three approaches, allowing our OAVI planner to run at up 15 Hz.

V. CONCLUSION

Approach	Planning Time
CSQMI	0.027 ± 0.02s
ROI-CSQMI	0.022 ± 0.02s
OAVI	0.036 ± 0.03s

TABLE II: Planning times onboard the robot’s computer during hardware experiments show the computational-efficiency of the proposed approach.

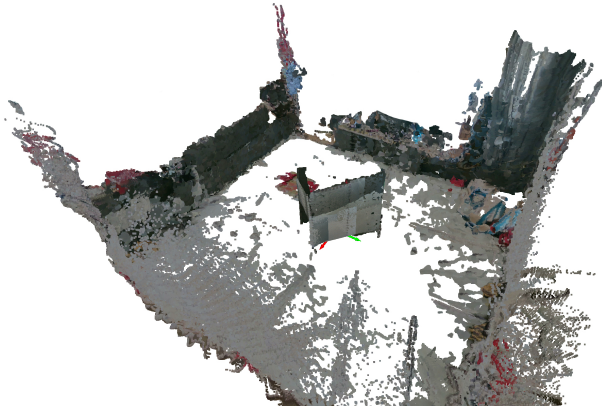


Fig. 10: Reconstructed point cloud map of the 50 m³ environment from the OAVI hardware trial.

This paper presented a methodology for collaborative human-robot exploration with implicit coordination. The approach developed in this work, OAVI, is an information-gain objective function inspired by active reconstruction techniques. The proposed approach was compared against an information-theoretic exploration baseline, CSQMI, and an extension to this baseline, ROI-CSQMI, which applies a spatial constraint to bias actions within the human’s FoV.

Comparing these approaches in simulation and hardware yields the following conclusions: (1) the baseline CSQMI approach is not well-suited to the collaboration paradigm detailed in this paper because it has no notion of the human’s ROI and cannot bias motion plans to reduce uncertainty towards the human’s FoV; (2) the ROI-CSQMI approach is ideal for a leader-follower exploration strategy because it selects motion plans that are restricted within the ROI; and (3) the OAVI approach is ideal for the collaborative human-robot exploration paradigm outlined in this paper because it causes the robot to select views within the ROI first and then explore outside the ROI when a sufficient number of views within the ROI have been collected.

In future work, we aim to deploy the exploration system for longer durations and with a moving human collaborator in outdoor, field environments. Further, we will relax assumptions on perfect knowledge of human-robot poses and their relative transforms in the world frame.

REFERENCES

[1] M. Tranzatto, F. Mascarich, L. Bernreiter, and C. Godinho et al., “Cerberus: Autonomous legged and aerial robotic exploration in the tunnel and urban circuits of the darpa subterranean challenge,” *Field Robotics*, vol. 2, pp. 274–324, 2022.

[2] S. Scherer, V. Agrawal, G. Best, C. Cao, K. Cujic, and R. Darnley et

al., “Resilient and modular subterranean exploration with a team of roving and flying robots,” *Field Robotics*, vol. 2, pp. 678–734, 2022.

[3] W. Tabib, K. Goel, J. Yao, M. Dabhi, C. Boirum, and N. Michael, “Real-time information-theoretic exploration with gaussian mixture model maps,” in *Robotics: Science and Systems*, 2019.

[4] V. Govindarajan, S. Bhattacharya, and V. Kumar, “Human-robot collaborative topological exploration for search and rescue applications,” in *DARS*. Springer, 2016, pp. 17–32.

[5] J. E. Domínguez-Vidal, I. J. Torres-Rodríguez, A. Garrell, and A. Sanfeliu, “User-friendly smartphone interface to share knowledge in human-robot collaborative search tasks,” in *2021 30th IEEE International Conference on Robot & Human Interactive Communication (RO-MAN)*. IEEE, 2021, pp. 913–918.

[6] M. Gu, E. Croft, and A. Cosgun, “Ar point&click: An interface for setting robot navigation goals,” *preprint arXiv:2203.15219*, 2022.

[7] S. Keshavdas and G.-J. M. Kruijff, “Functional mapping for human—robot collaborative exploration,” *International Journal of Computers and Applications*, vol. 35, no. 3, pp. 125–135, 2013.

[8] N. Wilde, A. Blidaru, S. L. Smith, and D. Kulić, “Improving user specifications for robot behavior through active preference learning: Framework and evaluation,” *The International Journal of Robotics Research*, vol. 39, no. 6, pp. 651–667, 2020.

[9] J. Delmerico, S. Isler, R. Sabzevari, and D. Scaramuzza, “A comparison of volumetric information gain metrics for active 3d object reconstruction,” *Autonomous Robots*, vol. 42, no. 2, pp. 197–208, 2018.

[10] W. Bentz, S. Dhanjal, and D. Panagou, “Unsupervised learning of assistive camera views by an aerial co-robot in augmented reality multitasking environments,” in *2019 International Conference on Robotics and Automation (ICRA)*. IEEE, 2019, pp. 3003–3009.

[11] C. Reardon, K. Lee, J. G. Rogers, and J. Fink, “Communicating via augmented reality for human-robot teaming in field environments,” in *2019 IEEE International Symposium on Safety, Security, and Rescue Robotics (SSRR)*. IEEE, 2019, pp. 94–101.

[12] B. Yamauchi, “Frontier-based exploration using multiple robots,” in *Proceedings of the second international conference on Autonomous agents*, 1998, pp. 47–53.

[13] W. Burgard, M. Moors, C. Stachniss, and F. E. Schneider, “Coordinated multi-robot exploration,” *IEEE Transactions on robotics*, vol. 21, no. 3, pp. 376–386, 2005.

[14] M. Dharmadhikari, H. Nguyen, F. Mascarich, N. Khedekar, and K. Alexis, “Autonomous cave exploration using aerial robots,” in *2021 International Conference on Unmanned Aircraft Systems (ICUAS)*. IEEE, 2021, pp. 942–949.

[15] Y. Nevatia, T. Stoyanov, R. Rathnam, M. Pfingsthorn, S. Markov, R. Ambrus, and A. Birk, “Augmented autonomy: Improving human-robot team performance in urban search and rescue,” in *2008 IEEE/RSJ IROS*. IEEE, 2008, pp. 2103–2108.

[16] F. Bourgault, A. A. Makarenko, S. B. Williams, B. Grocholsky, and H. F. Durrant-Whyte, “Information based adaptive robotic exploration,” in *2002 IEEE/RSJ IROS*, vol. 1. IEEE, 2002, pp. 540–545.

[17] B. J. Julian, S. Karaman, and D. Rus, “On mutual information-based control of range sensing robots for mapping applications,” *IJRR*, vol. 33, no. 10, pp. 1375–1392, 2014.

[18] B. Charrow, S. Liu, V. Kumar, and N. Michael, “Information-theoretic mapping using cauchy-schwarz quadratic mutual information,” in *2015 IEEE International Conference on Robotics and Automation (ICRA)*. IEEE, 2015, pp. 4791–4798.

[19] W. Tabib, K. Goel, J. Yao, C. Boirum, and N. Michael, “Autonomous cave surveying with an aerial robot,” *IEEE Transactions on Robotics*, pp. 1–17, 2021.

[20] K. Goel, W. Tabib, and N. Michael, “Rapid and high-fidelity subsurface exploration with multiple aerial robots,” in *Experimental Robotics*, B. Siciliano, C. Laschi, and O. Khatib, Eds. Cham: Springer International Publishing, 2021, pp. 436–448.

[21] J. I. Vazquez-Gomez, L. E. Sucar, R. Murrieta-Cid, and E. Lopez-Damian, “Volumetric next-best-view planning for 3d object reconstruction with positioning error,” *International Journal of Advanced Robotic Systems*, vol. 11, no. 10, p. 159, 2014.

[22] S. Kriegel, C. Rink, T. Bodenmüller, and M. Suppa, “Efficient next-best-scan planning for autonomous 3d surface reconstruction of unknown objects,” *Journal of Real-Time Image Processing*, vol. 10, no. 4, pp. 611–631, 2015.

[23] S. Thrun, “Probabilistic robotics,” *Communications of the ACM*, vol. 45, no. 3, pp. 52–57, 2002.

[24] T. Cover, *Elements of information theory*. John Wiley & Sons, 1999.